Fault estimation of wind turbines using combined adaptive and parameter estimation schemes

Marcin Witczak[1] | Damiano Rotondo[2,3] | Vicenç Puig[2,4] | Fatiha Nejjari[2] | Marcin Pazera[1]

[1]Institute of Control and Computation Engineering, University of Zielona Góra, ul. Podgórna 50, 65-246 Zielona Góra, Poland

[2]Automatic Control Department, Universitat Politècnica de Catalunya, Rambla de Sant Nebridi, 11 08222 Terrassa, Spain

[3]Centre for Autonomous Marine Operations and Systems, Department of Engineering Cybernetics, Norwegian University of Science and Technology, Trondheim, Norway

[4]Institut de Robòtica i Informàtica Industrial, UPC-CSIC, Carrer de Llorens i Artigas, 4-6 08028 Barcelona, Spain

Correspondence
Marcin Witczak, Institute of Control and Computation Engineering, University of Zielona Góra, ul. Podgórna 50, 65-246 Zielona Góra, Poland.
Email: m.witczak@issi.uz.zgora.pl

Funding information
National Science Centre in Poland, Grant/Award Number: 2013/11/B/ST7/01110; Spanish Ministry of Science and Technology, Grant/Award Number: DPI2014-58104-R; L′Agència de Gestió d′Ajuts Universitaris i de Recerca, Grant/Award Number: FI-DGR 2015, 2015FI_B2 00171; Direcció General de Recerca of Generalitat de Catalunya, Grant/Award Number: 2014/SGR/374; Research Council of Norway, Grant/Award Number: 223254; ERCIM Alain Bensoussan Fellowship Programme

Summary

This paper addresses the problem of fault estimation in wind turbines using a joint fault and state estimation scheme. The scheme assumes a set of possible faults affecting the dynamics of the wind turbine. Then, a combined adaptive and parameter estimation scheme is developed taking into consideration that process disturbances and sensor noises are unknown but bounded in an ellipsoid. Two subcases are considered depending on the satisfaction of a certain rank condition. The proposed approach is applied to a wind turbine based on a benchmark system model. The benchmark represents relevant fault scenarios, including sensor, actuator, and process faults. The proposed approach focuses on the last group of faults. Finally, the obtained results show that a satisfactory fault estimation is achieved against a set of predefined fault scenarios.

KEYWORDS

fault estimation, joint fault and state estimation, unknown-but-bounded uncertainty, wind turbine

1 | INTRODUCTION

Nowadays, the generation of electricity with wind turbines is a great success all over the world. Every year, new onshore and offshore wind farms are being deployed. All forecasts foresee that this evolution will continue in the forthcoming years. However,

wind turbines are complex systems that need to be maintained correctly. Moreover, because some of these wind turbines work in difficult meteorological conditions and the accessibility to perform maintenance is not easy and quite costly (especially those located offshore), there is an increasing need for enhancing the wind turbine control systems with fault-tolerant mechanisms that allow continuous operation of the wind turbine even in the event of a fault. This way, in a faulty case, the wind turbine can continue to operate without stopping the energy production, thus increasing their reliability.

For this reason, fault detection and isolation (FDI) and fault-tolerant control (FTC) with application to wind turbines have become a subject of increasing research interest both for the industry and the academia. In the light of such increased interest, researchers from the FDI/FTC community have proposed an international competition on FDI and FTC of wind turbines using a realistic wind turbine benchmark.[1,2] In the work of Odgaard et al,[3] a summary of the results obtained in this competition has been presented.

Until recent years, the application of advanced FDI algorithms in wind turbines was not so widespread. Most of the existing FDI applications were based on some form of signal analysis approach, as in the work of Johnson and Fleming.[4] For a review on the FDI techniques commonly used in industry, which are based on signal analysis, the reader is referred to the work of Hameed et al.[5] The overview of some FDI solutions is summarized in the work of Odgaard and Stoustrup.[6] Moreover, there were no FTC applications to wind turbines reported in the literature, so the common approach to deal with faults in the turbine was to shut it down if a fault was detected.[7]

Nowadays, a large number of FDI approaches for wind turbines are reported in the literature. Some of them were compared within the wind turbine FDI competition.[3] Most of these solutions rely on the evaluation of residuals to achieve FDI (see, eg, previous works[8-12] and the references therein). However, most of these approaches have focused on FDI, but not on fault estimation. Fault estimation is an important step to cover when thinking about the implementation of FTC. The knowledge about the fault size allows compensating the fault without removing the faulty component (sensor or actuator) and without the need for having hardware redundancy.

Most of the contributions regarding FTC assume that fault estimation is already available. In the work of Sloth et al,[13] a solution to this problem based on the design of passive and active FTC was proposed for a 4.8-MW variable-speed variable-pitch wind turbine model with a fault in the pitch system. In the case of active FTC, a linear parameter–varying gain-scheduling controller is developed using the fault estimation as the scheduling variable. However, the paper does not provide a mechanism for estimating the fault. In the work of Badihi et al,[14] a fuzzy gain-scheduled active FTC of a wind turbine is proposed. In the work of Kamal et al,[15] a multiobserver switching control strategy for robust active fuzzy FTC is proposed for variable-speed wind energy conversion systems subject to sensor faults.

Recently, some works have been dedicated to fault estimation for active FTC implementation. For example, in the work of Simani and Castaldi,[16] an active FTC scheme based on adaptive filters obtained via the nonlinear geometric approach is proposed. The controller accommodation scheme exploits the online estimate of the actuator fault signal generated by the adaptive filters. In the work of Blesa et al,[9] an FTC scheme based on virtual sensors and actuators is proposed, where the fault estimation is provided by a parameter estimation scheme. In the work of Shaker and Patton,[17] an active sensor fault-tolerant tracking control for offshore wind turbine described via Takagi-Sugeno multiple models is proposed. Because of the dependence of this strategy on the fault estimation, an observer with the capability to estimate a wide range of time-varying fault signals is used. In the work of Shi and Patton,[18] an observer-based descriptor system FTC scheme is designed for an offshore wind turbine system using a robust linear parameter–varying framework, where both the faults and the required states are estimated. In the work of Schulte and Gauterin,[19] a Takagi-Sugeno sliding mode observer for actuator fault diagnosis and an FTC scheme of wind turbines with hydrostatic transmission are presented. A simple compensation approach is implemented by subtracting the reconstructed faults obtained from the faulty inputs.

This paper addresses the problem of fault estimation in wind turbines using a combined adaptive and parameter estimation scheme and assuming that process disturbances and sensor noises are unknown but bounded in an ellipsoid. The scheme considers a set of possible faults affecting the dynamics of the wind turbine. Two subcases are considered depending on the satisfaction of a certain rank condition. Notice that in the proposed approach, FDI is performed by looking directly at the value of the estimated fault, differing from other approaches available in the literature, which aim at decoupling the disturbances and then exploiting the available degrees of freedom in the choice of the observer gains to provide fault-related directional properties to the output estimation error.[20] The proposed technique is applied to a well-known wind turbine benchmark and tested satisfactorily against a set of predefined fault scenarios.

The structure of the paper is as follows. The wind turbine benchmark and the considered fault scenarios are presented in Section 2. The proposed approach is presented in Section 3. Results of the application of the proposed scheme to the considered benchmark are presented in Section 4. In Section 5, the conclusions are given and future research directions are suggested.

2 | WIND TURBINE BENCHMARK DESCRIPTION

2.1 | Motivation

Wind turbines produce electrical energy using the kinetic energy of the wind. The wind turbine considered hereafter is the one proposed in the benchmark described in the work of Odgaard et al.[3] This turbine is a variable-speed, pitch-controlled, 3-blade horizontal-axis turbine with a full converter coupling. The pressure from the wind on the turbine blades forces the wind turbine rotor to spin around. Then, a rotating shaft converts the kinetic wind energy into mechanical energy. By pitching the blades or by controlling the rotational speed of the rotor with respect to the wind speed, the energy generation can be controlled. A generator, coupled to a converter, performs the conversion from mechanical energy to electrical energy (see previous works[21-23] for further details about the functioning of wind turbines).

The control system has the objective to follow the power reference or, alternatively, if the wind speed is too low, to achieve the desired power reference, to optimize the power production. The controller operates in 4 operational zones, governed by the mean wind speed within some time window. Zone 1 (turbine at standstill) and zone 4 (high wind speed, for which the energy production of the turbine must be stopped because of safety reasons) are not considered in the benchmark case study since its aim is to investigate fault detection under normal operation, which corresponds to zone 2 (power optimization due to partial load) and zone 3 (constant power production).

2.2 | Main sources of uncertainty and disturbance in wind turbines

Wind turbines are challenging systems for which robustness and fault-tolerance capabilities should be taken into account while designing control strategies. In fact, they are systems with complex dynamics that operate in uncertain environments where the wind conditions such as speed and direction are poorly known disturbances.[24] On the other hand, the aerodynamic properties of the blades are sensitive to atmospheric conditions,[25] leading to an uncertain behavior of this subsystem. In fact, the blade geometry will change because of the aging of the blade materials. Moreover, throughout the wind turbine's lifetime, the blades will suffer the effects of being exposed to the environment: change in blade surface roughness because of the layers of dirt formed by dust particles and insects and blade erosion because of the impact with objects or birds. In addition, some wind turbines are placed in locations where humidity and low temperatures are experienced during winters, and this increases the risk of ice accretion on wind turbine components,[26] which causes a reduction in the turbine power output.

2.3 | Wind turbine nonlinear model

Hereafter, the model of the wind turbine[1] is presented. The overall wind turbine is divided into appropriate submodels that are modeled separately. The system is driven by the wind speed that affects the aerodynamic properties of the wind turbine, together with the pitch angles of the blades and the speed of the rotor. An aerodynamic torque is transferred from the rotor to the generator through the drive train. Finally, the converter provides the electric power.

Drive train model: The drive train model consists of a low-speed shaft and a high-speed shaft having inertias J_r and J_g and friction coefficients B_r and B_g. The shafts are interconnected by transmission having a gear ratio N_g and efficiency η_{dt}, combined with torsion stiffness K_{dt}, and torsion damping B_{dt}. Thus, the drain train can be described by the following 3 differential equations[13]:

$$\dot{\omega}_r(t) = -\frac{(B_{dt} + B_r)}{J_r}\omega_r(t) + \frac{B_{dt}}{N_g J_r}\omega_g(t) - \frac{K_{dt}}{J_r}\theta_\Delta(t) + \frac{T_r(t)}{J_r} \tag{1}$$

$$\dot{\omega}_g(t) = \frac{\eta_{dt}B_{dt}}{N_g J_g}\omega_r(t) - \left(\frac{\eta_{dt}B_{dt}}{N_g^2 J_g} + \frac{B_g}{J_g}\right)\omega_g(t) + \frac{\eta_{dt}K_{dt}}{N_g J_g}\theta_\Delta(t) - \frac{T_g(t)}{J_g} \tag{2}$$

$$\dot{\theta}_\Delta(t) = \omega_r(t) - \frac{\omega_g(t)}{N_g}, \tag{3}$$

where ω_r is the rotor speed, ω_g is the generator speed, θ_Δ is the torsion angle of the drive train, T_r is the aerodynamic torque, and T_g is the generator torque. Both the rotor speed ω_r and the generator speed ω_g are measured.

Generator model: The generator torque T_g is controlled by the reference $T_{g,\text{ref}}$. The dynamics is approximated by a first-order model with time constant τ_g, as follows:

$$\dot{T}_g(t) = -\frac{T_g(t)}{\tau_g} + \frac{T_{g,\text{ref}}(t)}{\tau_g}. \tag{4}$$

TABLE 1 Values of the system parameters

Parameter	Value	Parameter	Value	Parameter	Value
J_r	$55{\cdot}10^6$ kg·m^2	η_{dt}	0.97	ω_{n0}	11.11 rad/s
J_g	390 kg·m^2	K_{dt}	$2.7{\cdot}10^9$ N·m/rad	ζ_0	0.6
B_r	7.11 N·m·s/rad	B_{dt}	775.49 N·m·s/rad	ρ	1.225 kg/m^3
B_{g0}	45.6 N·m·s/rad	τ_g	$20{\cdot}10^{-3}$ s	R	57.5 m
N_g	95	ω_{nf}	5.73 rad/s	ζ_f	0.45
		B_{gf}	68.4 N·m·s/rad		

Pitch system model: The hydraulic pitch system is modeled as a second-order system with input $\beta_{i,\text{ref}}$, natural frequency $\omega_{n,i}$, and damping ratio ζ_i,[27] as follows:

$$\ddot{\beta}_i(t) = -2\zeta_i\omega_{n,i}\dot{\beta}_i(t) - \omega_{n,i}^2\beta_i(t) + \omega_{n,i}^2\beta_{i,\text{ref}}(t), \tag{5}$$

where $i = 1, 2, 3$. The pitch angles $\beta_i(t)$, $i = 1, 2, 3$, are measured.

Aerodynamic model: The aerodynamics of the wind turbine is modeled as a torque acting on the blades. This aerodynamics torque $T_r(t)$ can be represented by[28]

$$T_r(t) = \sum_{i=1}^{3} \frac{\rho\pi R^3 C_q\left(\lambda(t), \beta_i(t)\right) v_w^2(t)}{6}, \tag{6}$$

where ρ is the air density, R is the radius of the blades, v_w is the wind speed, and C_q is the torque coefficient, which is a function of the pitch angle β_i and the tip speed ratio, defined as

$$\lambda(t) = \frac{\omega_r(t)R}{v_w(t)}. \tag{7}$$

The values of the system parameters used in this paper have been taken from the work of Odgaard and Johnson[2] and are presented in Table 1.

2.4 | Fault scenarios

In this paper, we focus on the faults in the pitch system and in the drive train to illustrate the proposed fault estimation approach.

The hydraulic pitch system can be affected by faults that change the dynamics because of either a drop in the hydraulic supply system, which can represent a leakage in the hose or a blocked pump, or high air content in the oil.[2]

In order to model this fault, let us introduce the fault effectiveness parameter $f_i(t)$, such that $f_i(t) = 0$ corresponds to the fault-free ith pitch system with $\omega_{n,i}^2 = \omega_{n0}^2$, $\zeta_i\omega_{n,i} = \zeta_0\omega_{n0}$, while $f_i(t) = 1$ corresponds to a full fault on the ith pitch system, such that $\omega_{n,i}^2 = \omega_{nf}^2$, $\zeta_i\omega_{n,i} = \zeta_f\omega_{nf}$.[18] Hence, both $\omega_{n,i}^2$ and $\zeta_i\omega_{n,i}$ can be described as a function of $f_i(t)$, as follows:

$$\omega_{n,i}^2 = (1 - f_i(t))\,\omega_{n0}^2 + f_i(t)\omega_{nf}^2 \tag{8}$$

$$\zeta_i\omega_{n,i} = (1 - f_i(t))\,\zeta_0\omega_{n0} + f_i(t)\zeta_f\omega_{nf}. \tag{9}$$

It is simple to check that Equation 5, together with Equations 8 and 9 and taking into account the available measurements, can be rewritten in state-space form as[18]

$$\begin{bmatrix}\dot{\beta}_i(t)\\ \ddot{\beta}_i(t)\end{bmatrix} = \begin{bmatrix}0 & 1\\ -\omega_{n0}^2 & -2\zeta_0\omega_{n0}\end{bmatrix}\begin{bmatrix}\beta_i(t)\\ \dot{\beta}_i(t)\end{bmatrix} + \begin{bmatrix}0\\ \omega_{n0}^2\end{bmatrix}\beta_{i,\text{ref}}(t) + \begin{bmatrix}0\\ 1\end{bmatrix}z_{\beta i}(t) \tag{10}$$

$$y_{\beta_i}(t) = \begin{bmatrix}1 & 0\end{bmatrix}\begin{bmatrix}\beta_i(t)\\ \dot{\beta}_i(t)\end{bmatrix}, \tag{11}$$

where

$$z_{\beta i}(t) = f_i(t)\left[\left(\omega_{n0}^2 - \omega_{nf}^2\right)\beta_i(t) + 2\left(\zeta_0\omega_{n0} - \zeta_f\omega_{nf}\right)\dot{\beta}_i(t) + \left(\omega_{nf}^2 - \omega_{n0}^2\right)\beta_{i,\text{ref}}(t)\right]. \tag{12}$$

In order to allow digital implementation of the joint state and fault estimation technique described in Section 3, Equations 10 and 11 are brought to a discrete-time form using a discretization method, eg, the Euler approach with sampling time T_s, obtaining

$$\begin{bmatrix}\beta_i(k+1)\\ \dot{\beta}_i(k+1)\end{bmatrix} = \begin{bmatrix}1 & T_s\\ -\omega_{n0}^2T_s & 1 - 2\zeta_0\omega_{n0}T_s\end{bmatrix}\begin{bmatrix}\beta_i(k)\\ \dot{\beta}_i(k)\end{bmatrix} + \begin{bmatrix}0\\ \omega_{n0}^2T_s\end{bmatrix}\beta_{i,\text{ref}}(k) + \begin{bmatrix}0\\ T_s\end{bmatrix}z_{\beta i}(k) \tag{13}$$

$$y_{\beta_i}(k) = \begin{bmatrix}1 & 0\end{bmatrix}\begin{bmatrix}\beta_i(k)\\ \dot{\beta}_i(k)\end{bmatrix}. \tag{14}$$

On the other hand, the fault in the drive train consists in a change of the high-speed shaft friction coefficient B_g, which is modeled by replacing B_{g0} by a lower value B_{gf}. Similarly to the pitch system case, let us introduce the parameter $f_g(t)$ such that

$$B_g = \left(1 - f_g(t)\right) B_{g0} + f_g(t) B_{gf}. \tag{15}$$

Hence, taking into account the available measurements, Equations 1 to 3 can be rewritten in state-space form as

$$\begin{bmatrix} \dot{\omega}_r(t) \\ \dot{\omega}_g(t) \\ \dot{\theta}_\Delta(t) \end{bmatrix} = \begin{bmatrix} -\frac{B_{dt}+B_r}{J_r} & \frac{B_{dt}}{N_g J_r} & -\frac{K_{dt}}{J_r} \\ \frac{\eta_{dt} B_{dt}}{N_g J_g} & -\left(\frac{\eta_{dt} B_{dt}}{N_g^2 J_g} + \frac{B_{g0}}{J_g}\right) & \frac{\eta_{dt} K_{dt}}{N_g J_g} \\ 1 & -\frac{1}{N_g} & 0 \end{bmatrix} \begin{bmatrix} \omega_r(t) \\ \omega_g(t) \\ \theta_\Delta(t) \end{bmatrix} + \begin{bmatrix} \frac{1}{J_r} & 0 \\ 0 & -\frac{1}{J_g} \\ 0 & 0 \end{bmatrix} \begin{bmatrix} T_r(t) \\ T_g(t) \end{bmatrix} + \begin{bmatrix} 0 \\ 1 \\ 0 \end{bmatrix} z_g(t) \tag{16}$$

$$y_{dt}(t) = \begin{bmatrix} 1 & 0 & 0 \\ 0 & 1 & 0 \end{bmatrix} \begin{bmatrix} \omega_r(t) \\ \omega_g(t) \end{bmatrix}, \tag{17}$$

where

$$z_g(t) = \frac{f_g(t)\left(B_{g0} - B_{gf}\right)}{J_g} \omega_g(t). \tag{18}$$

Also in this case, Equations 16 and 17 are brought to a discrete-time form using a Euler approach with sampling time T_s.

$$\begin{bmatrix} \omega_r(k+1) \\ \omega_g(k+1) \\ \theta_\Delta(k+1) \end{bmatrix} = \begin{bmatrix} 1 - T_s\frac{B_{dt}+B_r}{J_r} & T_s\frac{B_{dt}}{N_g J_r} & -T_s\frac{K_{dt}}{J_r} \\ T_s\frac{\eta_{dt} B_{dt}}{N_g J_g} & 1 - T_s\left(\frac{\eta_{dt} B_{dt}}{N_g^2 J_g} + \frac{B_{g0}}{J_g}\right) & T_s\frac{\eta_{dt} K_{dt}}{N_g J_g} \\ T_s & -\frac{T_s}{N_g} & 1 \end{bmatrix} \begin{bmatrix} \omega_r(k) \\ \omega_g(k) \\ \theta_\Delta(k) \end{bmatrix} + \begin{bmatrix} \frac{T_s}{J_r} & 0 \\ 0 & -\frac{T_s}{J_g} \\ 0 & 0 \end{bmatrix} \begin{bmatrix} T_r(k) \\ T_g(k) \end{bmatrix} + \begin{bmatrix} 0 \\ T_s \\ 0 \end{bmatrix} z_g(k) \tag{19}$$

$$y_{dt}(k) = \begin{bmatrix} 1 & 0 & 0 \\ 0 & 1 & 0 \end{bmatrix} \begin{bmatrix} \omega_r(k) \\ \omega_g(k) \end{bmatrix} \tag{20}$$

Remark 1. *Note that the pitch and drive train subsystems can be considered independently for the purpose of estimation of process faults. In fact, the pitch subsystem (13) and (14) is influenced neither by the state variables of the drive train subsystem nor by the drive train process fault. On the other hand, although it is true that a fault in the pitch subsystem will affect the drive train subsystem through the aerodynamics torque $T_r(t)$, it must be noted that $T_r(t)$ can be considered a known exogenous input for the purpose of state and process fault estimation, which means that the applicability of the proposed method will not be hindered by the interaction between the subsystems.*

3 | COMBINED ADAPTIVE AND PARAMETER ESTIMATION SCHEMES

As can be deduced from Equations 13 and 14, $z_{\beta_i}(k)$ $(i = 1, \ldots, 3)$ depends on both the known and unknown states and the faults. Thus, the idea is to first estimate $z_{\beta_i}(k)$ and the state variables. Note also that $z_{\beta_i}(k)$ depends linearly on fault $f_i(k)$. Thus, using the state estimates to form the regressor $\phi_i(k)$ (cf, Equation 12) and treating the estimate of $z_{\beta_i}(k)$ as an output of the following model:

$$\hat{z}_{\beta_i}(k) = \hat{f}_i(k)\phi_i(k), \tag{21}$$

the problem of estimating f_i can be formulated as a parameter estimation one. A similar analysis can be performed for Equations 19 and 20, while the problem boils down to estimating unknown states and $z_g(k)$. This results in

$$\hat{z}_g(k) = \hat{f}_g(k)\phi_g(k). \tag{22}$$

Finally, it should be pointed out that it is evident from either Equations 13 and 14 or Equations 19 and 20 that the direct estimation of faults is a nonlinear problem. The proposed 2-stage combined adaptive and parameter estimation scheme makes it possible to avoid this unappealing phenomenon. Indeed, the parameter estimation problem of Equation 21 or Equation 22 is to be solved with the well-known recursive least squares algorithm, while the adaptive estimators of the state and $\hat{z}_{\beta_i}(k)$ and $\hat{z}_g(k)$ are proposed in the sequel.

Thus, to simplify the notion and make it compatible with both Equations 13 and 14 and Equations 19 and 20, the following system description is introduced:

$$x(k+1) = Ax(k) + Bu(k) + Dz(k) + W_1 w_1(k) \tag{23}$$

$$y(k) = Cx(k) + W_2 w_2(k), \tag{24}$$

where $x \in \mathbb{R}^n$, $y \in \mathbb{R}^m$, and $u \in \mathbb{R}^r$ are the state, output, and input vectors, respectively, while $z \in \mathbb{R}^q$ stands for either $z_{\beta_i}(k)$ or $z_g(k)$. The matrix $D \in \mathbb{R}^{n\times q}$, with $rank(D) = q < n$, is denoted as the *fault distribution matrix* and describes the way in which the faults affect the system. Moreover, W_1 and W_2 denote the distribution matrices for the exogenous disturbances/noise w_1 and w_2, which affect the state and the output, respectively. Note that both Equations 13 and 14 and 19 and 20 can be rewritten in the form 23 and 24 by considering the presence of exogenous disturbances.

The problem is to design an estimator that is able to simultaneously estimate the state and the process fault. In the following, the proposed estimator will be called the *process fault estimator* (PFE). For the purpose of further developments, the following Assumptions are considered regarding the effect of faults, disturbances, and noises:

Assumption 1.

$$\varepsilon(k) \triangleq z(k+1) - z(k) \in \mathcal{E}_\varepsilon = \{\varepsilon : \varepsilon^T Q_\varepsilon \varepsilon \leq 1\}, \quad Q_\varepsilon \succ 0. \tag{25}$$

Assumption 2.

$$\begin{aligned} w_1(k) &\in \mathcal{E}_{w_1} = \left\{w_1 : w_1^T Q_{w_1} w_1 \leq 1\right\}, \quad Q_{w_1} \succ 0 \\ w_2(k) &\in \mathcal{E}_{w_2} = \left\{w_2 : w_2^T Q_{w_2} w_2 \leq 1\right\}, \quad Q_{w_2} \succ 0. \end{aligned} \tag{26}$$

Assumption 1 is required for the subsequent fault estimation algorithm. It has well-defined roots as all real faults and states are bounded, which means that $z(k)$ is bounded as well. Similarly, Assumption 2 states that the external disturbances are unknown but bounded. The diagonal elements of Q_ε correspond to constraints on the rate of change of $z(k)$, which means that the difference between consecutive samples of $z(k)$ must be bounded. Knowing that the state and fault are bounded, the bounds of $z(k)$ can be determined as well, which provides the settings of the diagonal elements of Q_ε. Similarly, having knowledge about the maximum values of external disturbances, the diagonal elements of Q_{w_1} and Q_{w_2} can be determined as well. The general idea behind this approach is that it provides knowledge about the upper and lower bounds of the external disturbances and faults that can be perceived as worst-case situations.

In the remainder of this section, 2 different estimators are proposed to solve the above-defined estimation problem, depending on whether or not the following condition holds true:

$$\text{rank}(CD) = \text{rank}(D) = q. \tag{27}$$

Note that the rank condition (27) does not hold for the pitch subsystem obtained from Equations 10 and 11. On the other hand, it holds true for the drive train subsystem obtained from Equations 16 and 17.

3.1 | Case 1: $rank(\boldsymbol{CD}) \neq rank(\boldsymbol{D})$

For this case, the following estimator is proposed:

$$\hat{x}(k+1) = A\hat{x}(k) + Bu(k) + D\hat{z}(k) + K\left(y(k) - C\hat{x}(k)\right) \tag{28}$$

$$\hat{z}(k+1) = \hat{z}(k) + L\left(y(k) - C\hat{x}(k)\right), \tag{29}$$

where $K \in \mathbb{R}^{n\times m}$ and $L \in \mathbb{R}^{q\times m}$ are gains to be designed.

From Equations 23 and 24, the evolution of the state estimation error $e(k) \triangleq x(k) - \hat{x}(k)$ is described by

$$e(k+1) = (A - KC)\, e(k) + De_z(k) + W_1 w_1(k) - KW_2 w_2(k), \tag{30}$$

where $e_z(k) \triangleq z(k) - \hat{z}(k)$.

Subsequently, the dynamics of the fault estimation error $e_z(k)$ is given by

$$\begin{aligned} e_z(k+1) &= z(k+1) + z(k) - z(k) - \hat{z}(k+1) = \varepsilon(k) + z(k) - \hat{z}(k+1) \\ &= \varepsilon(k) + z(k) - \hat{z}(k) - LCx(k) - LW_2 w_2(k) + LC\hat{x}(k) \\ &= \varepsilon(k) + e_z(k) - LCe(k) - LW_2 w_2(k), \end{aligned} \tag{31}$$

where $\varepsilon(k)$ is as defined in Equation 25.

By introducing the following vectors:

$$\bar{e}(k) = \left[\, e(k)^T, e_z(k)^T \,\right]^T \tag{32}$$

$$v(k) = \left[\, w_1(k)^T, w_2(k)^T, \varepsilon(k)^T \,\right]^T, \tag{33}$$

the state and fault estimation error dynamics are given by

$$\bar{e}(k+1) = \begin{bmatrix} A - KC & D \\ -LC & I \end{bmatrix} \bar{e}(k) + \begin{bmatrix} W_1 & -KW_2 & 0 \\ 0 & -LW_2 & I \end{bmatrix} v(k) \tag{34}$$

which can be described in an equivalent form

$$\bar{e}(k+1) = X\bar{e}(k) + Zv(k), \tag{35}$$

where

$$X = \bar{A} - \bar{K}\bar{C} = \begin{bmatrix} A & D \\ 0 & I \end{bmatrix} - \begin{bmatrix} K \\ L \end{bmatrix} \begin{bmatrix} C & 0 \end{bmatrix} \tag{36}$$

$$Z = \bar{W} - \bar{K}\bar{V} = \begin{bmatrix} W_1 & 0 & 0 \\ 0 & 0 & I \end{bmatrix} - \begin{bmatrix} K \\ L \end{bmatrix} \begin{bmatrix} 0 & W_2 & 0 \end{bmatrix}. \tag{37}$$

The ellipsoidal set including $v(k)$ can be described by

$$\mathcal{E}_v = \{v : v^T Q_v v \leq 1\}, \tag{38}$$

where

$$Q_v = \frac{1}{3}\text{diag}(Q_{w_1}, Q_{w_2}, Q_\varepsilon). \tag{39}$$

Note that, if $v(k) = 0$, then the usual Lyapunov approach can be used to prove the asymptotic convergence of $\bar{e}(k)$. However, if $v(k) \neq 0$, then such approach cannot be applied directly. Thus, for the purpose of further deliberations, the so-called quadratic boundedness[29-31] approach is used. To do so, let us define the Lyapunov function

$$V(k) = \bar{e}(k)^T P \bar{e}(k), \tag{40}$$

with $P \succ 0$, and let us be reminded of the following Definitions.[29-31]

Definition 1. *The system (35) is strictly quadratically bounded for all allowable $v \in \mathcal{E}_v$ if $\bar{e}(k)^T P \bar{e}(k) > 1$ implies $\bar{e}(k+1)^T P \bar{e}(k+1) < \bar{e}(k)^T P \bar{e}(k)$ for any $v(k) \in \mathcal{E}_v$.*

It should be highlighted that the strict quadratic boundedness of Equation 35 ensures that $V(k+1) < V(k)$ for any $v \in \mathcal{E}_v$ when $V(k) > 1$.

Definition 2. *A set $\mathcal{E}$ is a positively invariant set for Equation 35 for all $v \in \mathcal{E}_v$ if $\bar{e}(k) \in \mathcal{E}$ implies $\bar{e}(k+1) \in \mathcal{E}$ for any $v(k) \in \mathcal{E}_v$*

On the basis of these Definitions and the results presented in the work of Alessandri et al,[29] the following Lemma can be formulated for Equation 35:

Lemma 1. *The following statements are equivalent[29-31]:*

1. *The system (35) is strictly quadratically bounded for all $v \in \mathcal{E}_v$.*
2. *The ellipsoid*

$$\mathcal{E} = \{\bar{e} : \bar{e}^T P \bar{e} \leq 1\}, \tag{41}$$

   is an invariant set for Equation 35 for any $v \in \mathcal{E}_v$.
3. *There exists a scalar $\alpha \in (0, 1)$ such that*

$$\begin{bmatrix} X^T P X - P + \alpha P & X^T P Z \\ Z^T P X & Z^T P Z - \alpha Q_v \end{bmatrix} \preceq 0. \tag{42}$$

To provide the final design procedure, the following Theorem is proposed:

Theorem 1. *The system (35) is strictly quadratically bounded for all $v \in \mathcal{E}_v$ if there exist matrices $P \succ 0$, U and a scalar $\alpha \in (0, 1)$ such that the following inequality is satisfied:*

$$\begin{bmatrix} -P + \alpha P & 0 & \bar{A}^T P - \bar{C}^T U^T \\ 0 & -\alpha Q_v & \bar{W}^T P - \bar{V}^T U^T \\ P\bar{A} - U\bar{C} & P\bar{W} - U\bar{V} & -P \end{bmatrix} \preceq 0. \tag{43}$$

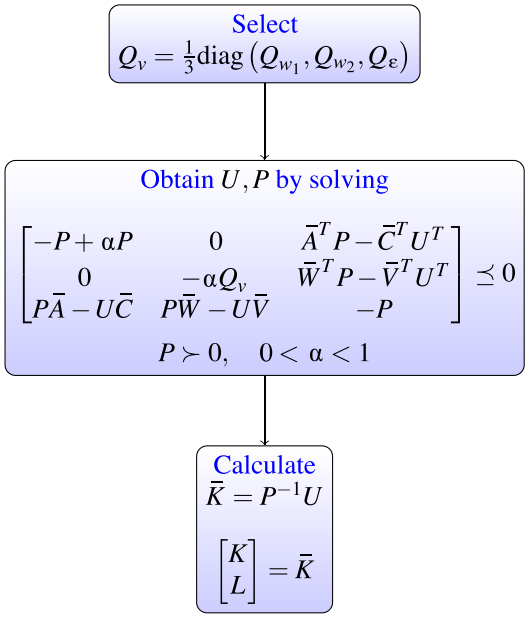

FIGURE 1 Process fault estimator design procedure for Case 1. [Colour figure can be viewed at wileyonlinelibrary.com]

Proof. *Inequality (42) can be rewritten into the following form:*

$$\begin{bmatrix} X^T \\ Z^T \end{bmatrix} P \begin{bmatrix} X & Z \end{bmatrix} + \begin{bmatrix} -P+\alpha P & 0 \\ 0 & -\alpha Q_v \end{bmatrix} \preceq 0. \tag{44}$$

Then, using the Schur complement and multiplying the left and right sides by diag(I, I, P) gives

$$\begin{bmatrix} -P+\alpha P & 0 & X^T P \\ 0 & -\alpha Q_v & Z^T P \\ PX & PZ & -P \end{bmatrix} \preceq 0. \tag{45}$$

Substituting

$$PX = P\bar{A} - P\bar{K}\bar{C} = P\bar{A} - U\bar{C} \tag{46}$$

$$PZ = P\bar{W} - P\bar{K}\bar{V} = P\bar{W} - UV \tag{47}$$

and introducing Equations 46 and 47 into Equation 45 completes the proof. □

Finally, the design procedure boils down to solving Equation 43 and then calculating

$$\bar{K} = \begin{bmatrix} K \\ L \end{bmatrix} = P^{-1}U. \tag{48}$$

A complete design procedure of the PFE is depicted in Figure 1.

3.2 | Case 2: *rank*(***CD***) = *rank*(***D***)

In this case, by combining Equations 23 and 24, the following result is obtained:

$$CDz(k) = y(k+1) - CAx(k) - CBu(k) - CW_1 w_1(k) - W_2 w_2(k+1), \tag{49}$$

which is an identity, since for given vectors $z(k)$, $x(k)$, $u(k)$, $w_1(k)$, and $w_2(k)$, the value of the vector $y(k+1)$ cannot be arbitrary, but is determined by Equations 23 and 24. It follows that if $z(k)$ is considered unknown, the linear system of equations resulting from Equation 49 would admit a solution (ie, the actual value of $z(k)$), which could be obtained as follows:

$$z(k) = H\left[y(k+1) - CAx(k) - CBu(k) - CW_1 w_1(k) - W_2 w_2(k+1)\right], \tag{50}$$

where

$$H = (CD)^\dagger = \left[(CD)^T CD\right]^{-1}(CD)^T, \tag{51}$$

where † denotes the Moore-Penrose pseudoinverse. Because of the rank condition (27), Equation 50 is the unique solution of the linear system obtained from Equation 49.

By substituting Equation 50 into Equation 23, it can be shown that

$$x(k+1) = \bar{A}x(k) + \bar{B}u(k) + \bar{H}y(k+1) + \bar{W}_1 w_1(k) + \bar{W}_2 w_2(k+1), \tag{52}$$

where

$$\bar{A} = (I - DHC)\,A \tag{53}$$

$$\bar{B} = (I - DHC)\,B \tag{54}$$

$$\bar{H} = DH \tag{55}$$

$$\bar{W}_1 = (I - DHC)\,W_1 \tag{56}$$

$$\bar{W}_2 = -DHW_2. \tag{57}$$

On the basis of Equations 50 and 52, the following estimator is proposed:

$$\hat{x}(k+1) = \bar{A}\hat{x}(k) + \bar{B}u(k) + \bar{H}y(k+1) + K\left(y(k) - C\hat{x}(k)\right) \tag{58}$$

$$\hat{z}(k) = H\left(y(k+1) - CA\hat{x}(k) - CBu(k)\right), \tag{59}$$

where $K \in \mathbb{R}^{n\times m}$ is the gain to be designed.

Then, the associated state estimation error is given by

$$e(k+1) = \left(\bar{A} - KC\right)e(k) + \bar{W}_1 w_1(k) - KW_2 w_2(k) + \bar{W}_2 w_2(k+1), \tag{60}$$

while the fault estimation error is described by

$$e_z(k) = -HCAe(k) - HCW_1 w_1(k) - HCW_2 w_2(k+1). \tag{61}$$

From Equations 60 and 61, it can be seen that the dynamics of $e(k)$ does not depend on $e_z(k)$, while at the same time there exists a static relationship between $e(k)$, $w_1(k)$, $w_2(k+1)$, and $e_z(k)$.

For this reason, to design the gain K, the quadratic boundedness–based procedure previously described can be applied, starting from Equation 35, but using

$$\bar{e}(k) = e(k) \tag{62}$$

$$v(k) = \left[w_1(k)^T, w_2(k)^T, w_2(k+1)^T\right]^T \tag{63}$$

$$X = \bar{A} - KC \tag{64}$$

$$Z = \begin{bmatrix} \bar{W}_1 & 0 & \bar{W}_2 \end{bmatrix} - K \begin{bmatrix} 0 & W_2 & 0 \end{bmatrix} \tag{65}$$

$$Q_v = \frac{1}{3}\mathrm{diag}\left(Q_{w_1}, Q_{w_2}, Q_{w_2}\right). \tag{66}$$

The final design procedure is summarized in Figure 2.

Remark 2. *It can be seen from Equation 59 that the estimated process fault vector $\hat{z}(k)$ is calculated using the measurement y at the following sample. From a practical perspective, this means that at sample k, when the value $y(k)$ is obtained, the proposed estimator will calculate $\hat{z}(k-1)$. This fact must be taken into account in case the estimated process fault vector is fed to a controller, eg, by relying on the available results for the analysis and control of systems affected by delays.*[32]

Remark 3. *The proposed design approach based on the notion of quadratic boundedness can be easily merged with other performances, obtaining a multiobjective design procedure similar to the one described in the work of Scherer et al.*[33] *As a matter of example, a $\mathcal{H}_\infty$ performance specification can be added to decrease the effect of the disturbances on the fault/state estimation.*

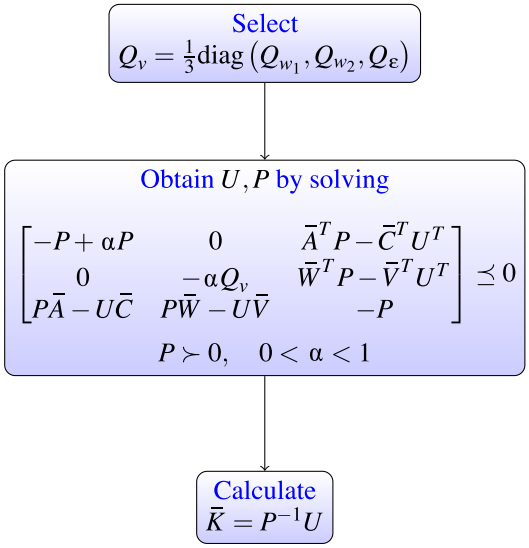

FIGURE 2 Process fault estimator design procedure for Case 2. [Colour figure can be viewed at wileyonlinelibrary.com]

3.3 | Fault effectiveness estimation

Note that the joint estimation of state and fault variables x and z also allows estimating the fault effectiveness parameters. In fact, by using the estimates $\hat{\beta}_i(k)$, $\hat{\dot{\beta}}_i(k)$, and $\hat{z}_{\beta_i}(k)$, the estimation $\hat{f}_i(k)$ can be extracted from Equation 12 using parameter estimation techniques, such as least squares methods.[34] In the same way, by using the estimates $\hat{\omega}_g(k)$ and $\hat{z}_g(k)$, a value $\hat{f}_g(k)$ can be extracted from Equation 18.

More specifically, the following regression equation can be derived from Equation 12:

$$z_{\beta_i}(k) = \phi_i(k) f_i(k), \tag{67}$$

by considering

$$\phi_i(k) = \left(\omega_{n0}^2 - \omega_{nf}^2\right)\beta_i(k) + 2\left(\zeta_0\omega_{n0} - \zeta_f\omega_{nf}\right)\dot{\beta}_i(k) + \left(\omega_{nf}^2 - \omega_{n0}^2\right)\beta_{i,\text{ref}}(k). \tag{68}$$

Then, by replacing $z_{\beta_i}(k)$, $\beta_i(k)$, $\dot{\beta}_i(k)$ with $\hat{z}_{\beta_i}(k)$, $\hat{\beta}_i(k)$, $\hat{\dot{\beta}}_i(k)$ (the resulting $\phi_i(k)$ will be denoted by $\hat{\phi}_i(k)$) and taking into account that ω_{n0}, ω_{nf}, ζ_0, ζ_f, and $\beta_{i,\text{ref}}(k)$ are known, Equation 67 becomes an equation where the only unknown parameter is $f_i(k)$, which can be estimated using parameter estimation methods. For example, a recursive least squares filter with a forgetting factor σ can be used to minimize a weighted linear least squares cost function related to the signals $\hat{z}_{\beta_i}(k)$ and $\hat{\phi}_i(k)$,[35] with the advantage of fast convergence that can be tuned through an appropriate choice of σ (the smaller σ is, the more sensitive is the filter to recent samples, which means faster convergence, but also more fluctuations because of disturbances and noise).

A similar reasoning can be applied to the drive train, in which case the regression equation

$$z_g(k) = \phi_g(k) f_g(k) \tag{69}$$

is obtained from Equation 18.

Remark 4. *In order to obtain a good estimation of the fault effectiveness signals $f_i(k)$ and $f_g(k)$, it would be desirable if the signals $\hat{z}_{\beta_i}(k)$ and $\hat{z}_g(k)$ took values different from 0 only when a fault is affecting the signal, ie, $f_i(k) \neq 0$ or $f_g(k) \neq 0$, respectively. In practice, this will not happen because of the presence of disturbances and noise, which will affect $\hat{z}_{\beta_i}(k)$ and $\hat{z}_g(k)$. However, under the assumption that the fault effect on the estimation is much stronger than the one due to disturbances and noise, it is possible to enhance the performance of the fault effectiveness estimator by using a threshold-filtered estimated signal $\hat{z}_{filt.}$ instead of the estimated signal $\hat{z}$ ($\hat{z} = \hat{z}_{\beta_i}$ or $\hat{z} = \hat{z}_g$ depending on the considered subsystem). In particular, $\hat{z}_{filt.}$ is defined as follows:*

$$\hat{z}_{filt.}(k) = \begin{cases} \hat{z}(k), & \text{if } \hat{z}(k) \geq \hat{z}_{th} \\ 0, & \text{else} \end{cases}, \tag{70}$$

where $\hat{z}_{th}$ is an appropriate threshold, which should be selected in such a way that only the values of $\hat{z}(k)$ that are not excited by the fault are filtered.

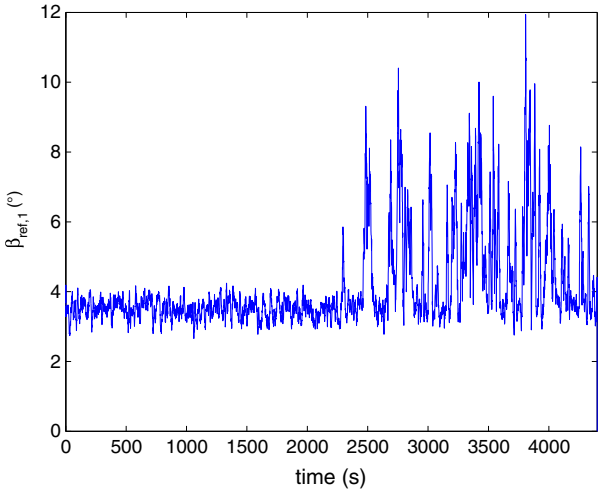

FIGURE 3 Reference for pitch system 1: $\beta_{1,\text{ref}}$. [Colour figure can be viewed at wileyonlinelibrary.com]

3.4 | Robustness analysis

The aim of this section is to provide a robustness metric that can be used for analyzing the performance of the PFE in the presence of model-reality mismatch. The proposed metric is based on the idea of stochastic robustness, which was first used by Marrison and Stengel[36] for designing robust control systems and later applied by Witczak and Pretki[37] to the design of unknown input observers. The robustness metric is given by the probability that the PFE will have an unacceptable performance in the presence of possible variations of the model. More specifically, let us denote the PFE by $\mathcal{E}(p)$, where p are the design parameters (the gains K and L, the forgetting factor σ, and the threshold $\hat{z}_{\text{th}}$), while the system will be denoted by $\mathcal{S}(\mu)$, where $\mu \in \mathbb{M}$ are the possible model variations due to the uncertainty, described by a probability density function $pr(\mu)$. Then, the robustness metric can be defined as the integral of an indicator function over the space of expected variations of the model, ie,

$$\Psi(p) = \int_{\mathbb{M}} I\left[\mathcal{S}(\mu), \mathcal{E}(p)\right] pr(\mu) d\mu, \tag{71}$$

where $I[\cdot,\cdot]$ is a binary indicator function that indicates if the performance of the PFE for a given realization of μ is acceptable or not. For example, the binary indicator function can be related to the mean-squared error (MSE) fault estimation error, as follows:

$$I\left[S(\mu), E(p)\right] = \begin{cases} 0, & \text{if } \frac{1}{N}\sum_{k=1}^{N}\left(f(k) - \hat{f}(k)\right)^2 \leq \varphi \\ 1, & \text{otherwise} \end{cases}, \tag{72}$$

where N denotes the number of samples and $\varphi > 0$ is the acceptable MSE. Note that alternative binary indicator functions can be employed, eg, the one based on an empirical evaluation of false alarms and missed fault rates.[38]

Unfortunately, Equation 71 cannot be integrated analytically. A practical alternative is to use Monte Carlo methods[39] with $pr(\mu)$ shaping random values of μ, which will be denoted by μ_i. When M random μ_i, $i = 1, \ldots, M$, are generated, then an estimate of Ψ is given by

$$\hat{\Psi}(p) = \frac{1}{M}\sum_{i=1}^{M} I\left[\mathcal{S}(\mu_i), \mathcal{E}(p)\right], \tag{73}$$

where $\hat{\Psi}$ approaches Ψ in the limit as $M \to \infty$. However, since it is impossible to set $M = \infty$, the problem boils down to selecting M in such a way that $\hat{\Psi}$ has a standard deviation less than a desired value $\sigma_{\hat{\Psi}}$. Since I in Equation 72 is binary, $\hat{\Psi}$ has a binomial distribution, such that following the reasoning detailed in the work of Witczak and Pretki,[37] M can be chosen as

$$M = \left\lceil \frac{1}{4}\sigma_{\hat{\Psi}}^{-2} \right\rceil. \tag{74}$$

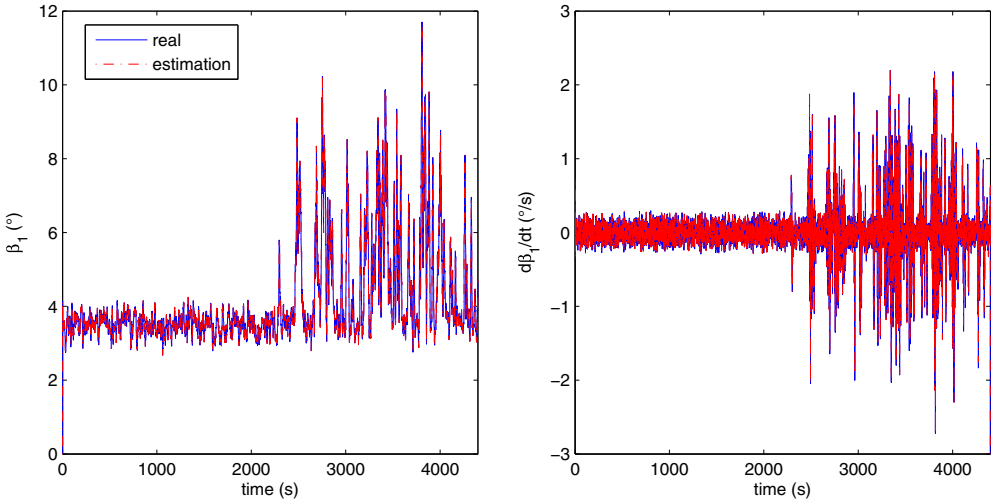

FIGURE 4 Pitch system 1: state variables β_1 and $\dot{\beta}_1$ (real vs estimation). [Colour figure can be viewed at wileyonlinelibrary.com]

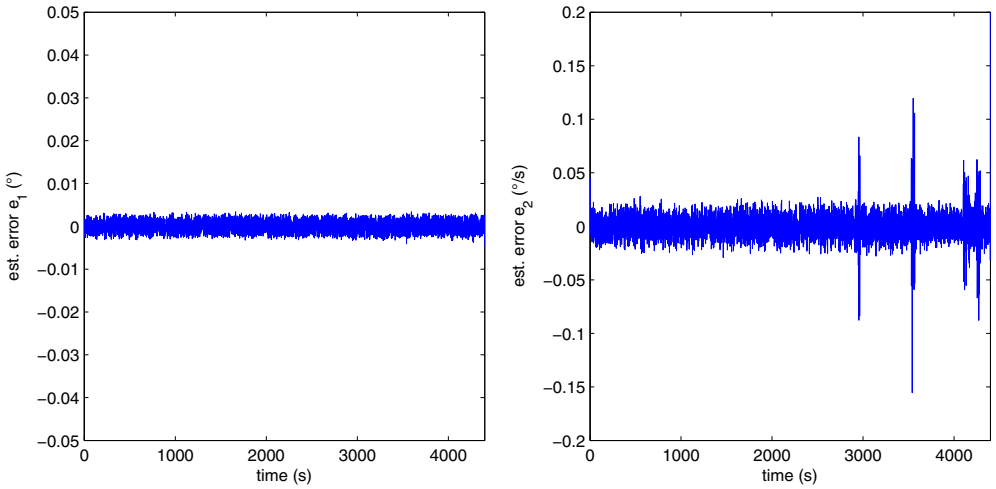

FIGURE 5 Estimation errors $e_1 = \beta_1 - \hat{\beta}_1$, $e_2 = \dot{\beta}_1 - \hat{\dot{\beta}}_1$. [Colour figure can be viewed at wileyonlinelibrary.com]

4 | APPLICATION TO THE WIND TURBINE CASE STUDY

4.1 | Fault scenario 1: faults in the pitch subsystem

First of all, let us evaluate the effectiveness of the PFE described in Section 3.1, ie, for the case where Equation 27 does not hold, by considering faults affecting the pitch system, as described in Section 2.4.

The design procedure described in Section 3.1 has been applied to the discrete-time model (13) and (14) with sampling time $T_s = 0.01$ seconds.

The exogenous disturbance distribution matrices are considered as follows:

$$W_1 = \begin{bmatrix} 1 \\ 0 \end{bmatrix} \quad W_2 = 1,$$

while the matrices Q_ε, Q_{w_1}, and Q_{w_2} are

$$Q_{w_1} = 1000 \quad Q_{w_2} = 10^6 \quad Q_\varepsilon = 100.$$

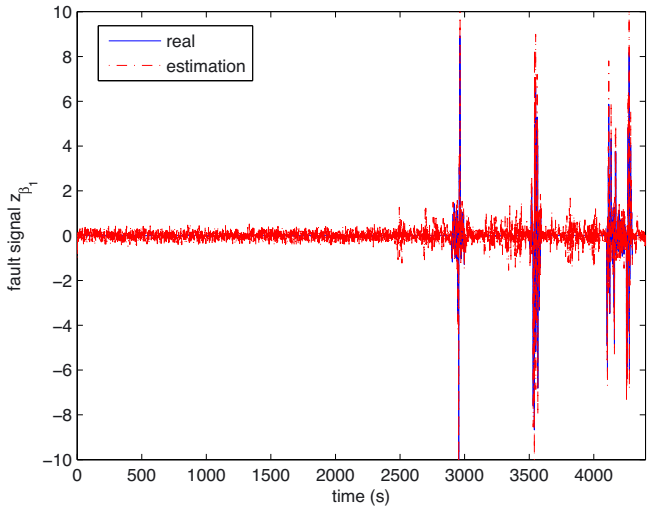

FIGURE 6 Fault signal z_{β_1} (real vs estimation). [Colour figure can be viewed at wileyonlinelibrary.com]

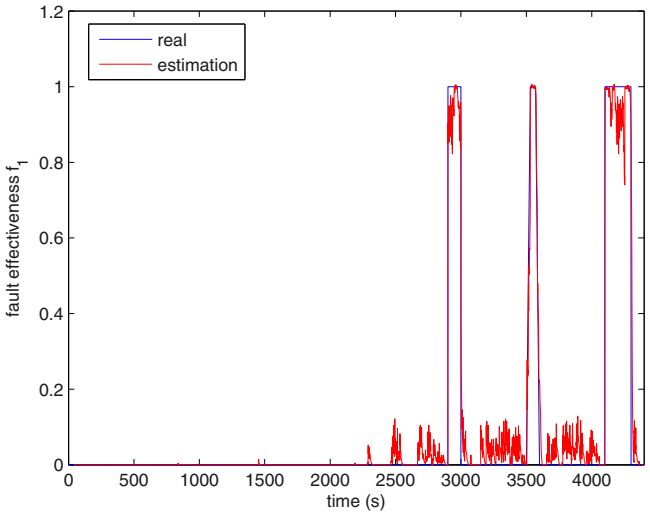

FIGURE 7 Fault effectiveness f_1 (real vs estimation). [Colour figure can be viewed at wileyonlinelibrary.com]

Theorem 1 has been applied for designing the gains K and L, with a value $\alpha = 0.1$, obtaining

$$P = 10^3 \begin{bmatrix} 1.8242 & -0.0397 & -0.0052 \\ -0.0397 & 0.0829 & -0.0049 \\ -0.0052 & -0.0049 & 0.0004 \end{bmatrix}$$

$$K = \begin{bmatrix} 0.7843 \\ 4.7511 \end{bmatrix} \quad L = 88.2718.$$

In order to assess the performance of this observer, the following evolution of the signal $f_1(t)$ (fault in the first pitch system) has been considered:

$$f_1(t) = \begin{cases} 1, & 2900 \text{ s} < t \leq 3000 \text{ s} \\ \frac{t-3500}{30}, & 3500 \text{ s} < t \leq 3530 \text{ s} \\ 1, & 3530 \text{ s} < t \leq 3570 \text{ s} \\ \frac{3600-t}{30}, & 3570 \text{ s} < t \leq 3600 \text{ s} \\ 1, & 4100 \text{ s} < t \leq 4300 \text{ s} \\ 0, & \text{else} \end{cases}, \tag{75}$$

which contains both abrupt and incipient faults.

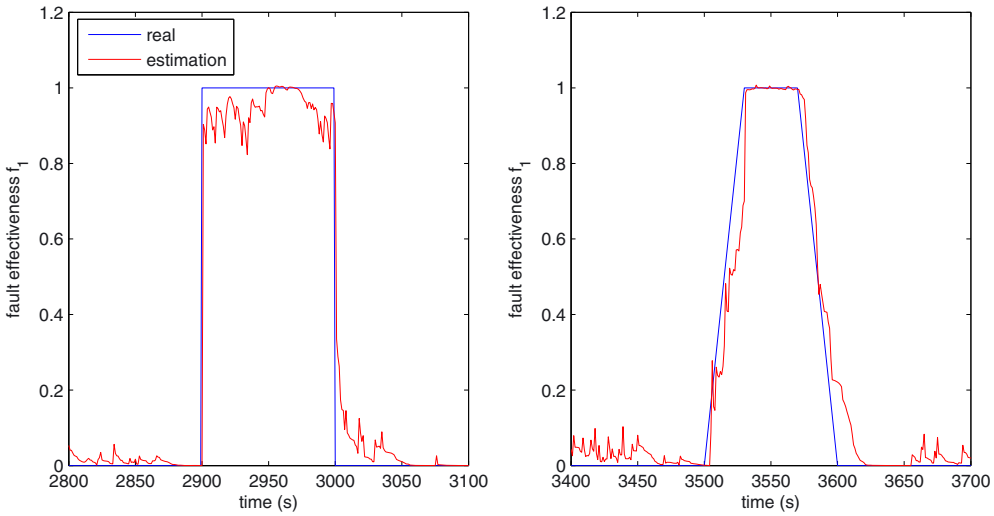

FIGURE 8 Fault effectiveness f_1 (real vs estimation, zoom). [Colour figure can be viewed at wileyonlinelibrary.com]

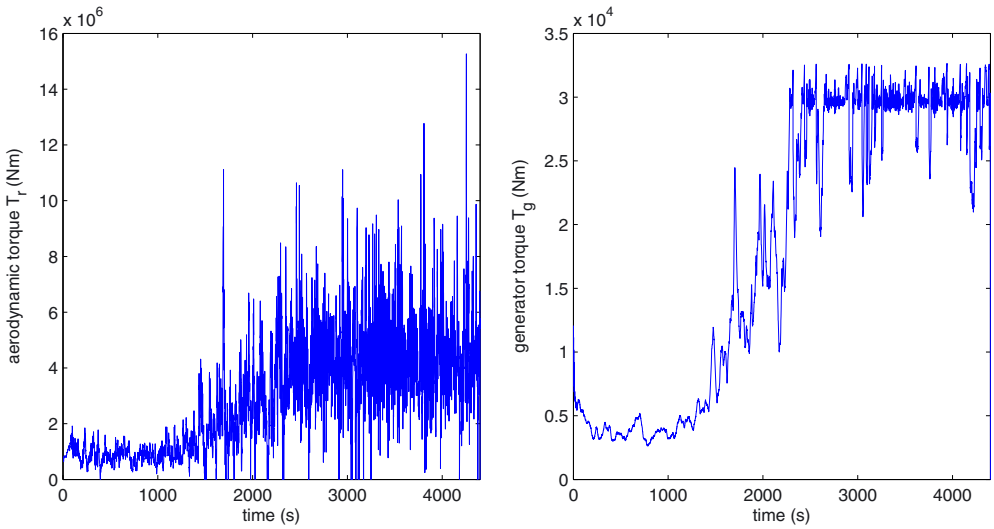

FIGURE 9 Inputs for the drive train subsystem: T_r and T_g. [Colour figure can be viewed at wileyonlinelibrary.com]

The results shown hereafter refer to a simulation that lasts 4400 seconds, where the input for the first pitch system $\beta_{\text{ref},1}(t)$ is as depicted in Figure 3.

Figure 4 shows the evolution of the state variables $\beta_1(t)$ and $\dot{\beta}_1(t)$ and their estimation using the designed observer. On the other hand, Figure 5 shows the estimation errors for both the state variables $\beta_1(t)$ and $\dot{\beta}_1(t)$. It can be seen that the designed observer is able to estimate correctly the state, although its effectiveness is affected by the presence of faults.

Figure 6 compares the fault signal $z_{\beta_1}(t)$ with its estimation. It can be seen that $\hat{z}_{\beta_1}$ is affected by the presence of exogenous disturbances even when no fault acts on the system. This motivates the introduction of a threshold-based filtering, which returns $\hat{z}_{\beta_1,\text{filt.}}$, obtained with Equation 70 and $\hat{z}_{\text{th}} = 0.6$.

Then, the recursive least squares approach with a forgetting factor of 0.997 is applied using Equation 12, obtaining the estimation of the fault effectiveness parameter $\hat{f}_1$, which is shown in Figures 7 and 8. Taking into account the presence of external disturbances, noise, and discretization errors, the obtained estimation is considered to be satisfactorily accurate.

4.2 | Fault scenario 2: faults in the drive train subsystem

Let us now evaluate the effectiveness of the PFE described in Section 3.2, ie, for the case where Equation 27 holds, by considering faults affecting the drive train subsystem, as described in Section 2.4.

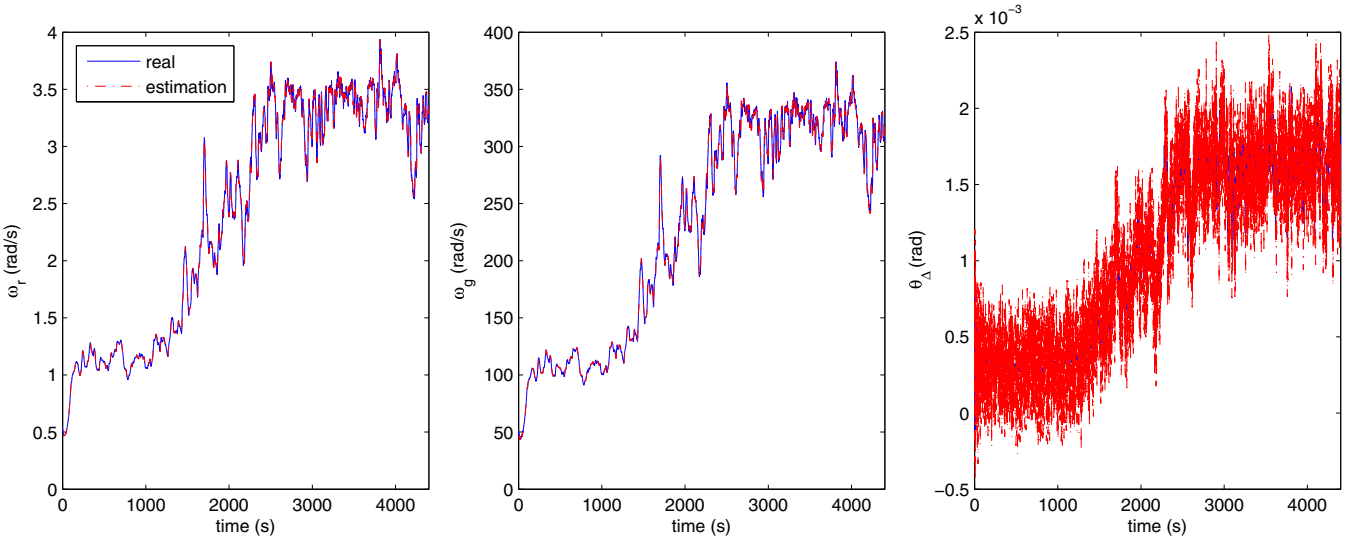

FIGURE 10 Drive train subsystem: state variables ω_r, ω_g, and θ_Δ (real vs estimation). [Colour figure can be viewed at wileyonlinelibrary.com]

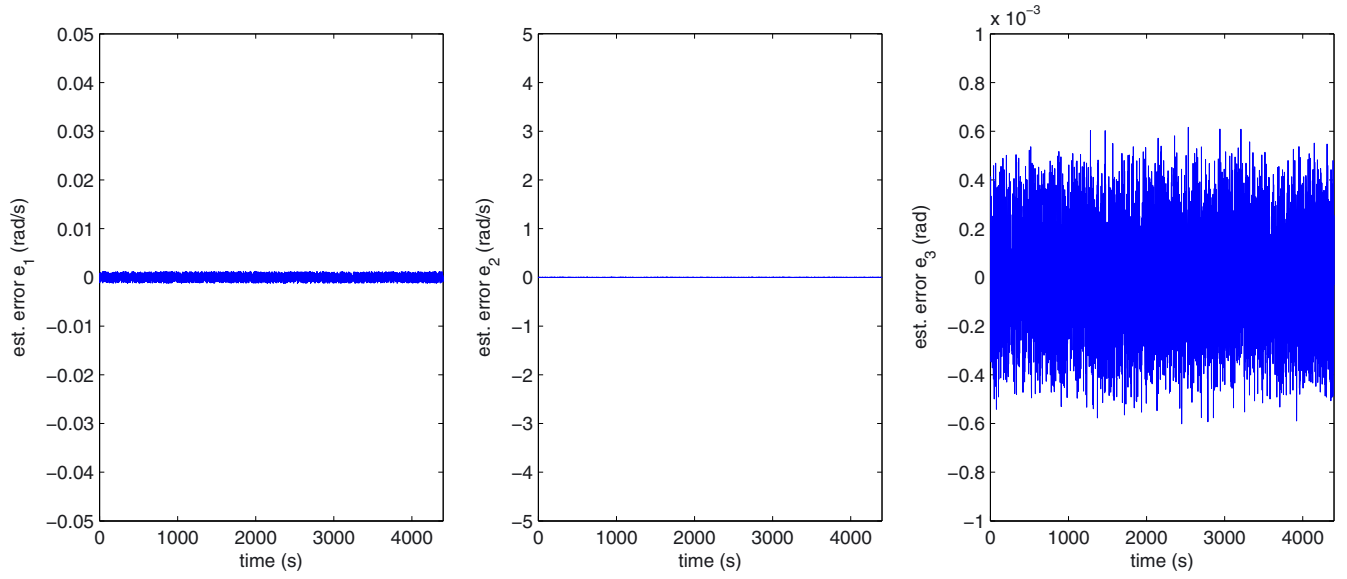

FIGURE 11 Estimation errors $e_1 = \omega_r - \hat{\omega}_r$, $e_2 = \omega_g - \hat{\omega}_g$, and $e_3 = \theta_\Delta - \hat{\theta}_\Delta$. [Colour figure can be viewed at wileyonlinelibrary.com]

The design procedure described in Section 3.2 has been applied to the discrete-time model (19) and (20) with sampling time $T_s = 0.01$ seconds.

The exogenous disturbance matrices are considered as follows:

$$W_1 = \begin{bmatrix} 1 & 0 \\ 0 & 1 \\ 0 & 0 \end{bmatrix} \quad W_2 = \begin{bmatrix} 1 & 0 \\ 0 & 1 \end{bmatrix},$$

while the matrices Q_{w_1} and Q_{w_2} are

$$Q_{w_1} = \begin{bmatrix} 10^8 & 0 \\ 0 & 5 \cdot 10^8 \end{bmatrix} \quad Q_{w_2} = \begin{bmatrix} 10^6 & 0 \\ 0 & 10^6 \end{bmatrix}.$$

Theorem 1 has been applied for designing the gain K, with a value $\alpha = 0.1$, obtaining

$$P = 10^4 \cdot \begin{bmatrix} 0.3364 & 0.3916 & 0.1799 \\ 0.3916 & 3.1667 & 0.1778 \\ 0.1799 & 0.1778 & 0.4687 \end{bmatrix} \quad K = \begin{bmatrix} 1.1843 & 0.9086 \\ -0.0036 & -0.0485 \\ -0.4081 & -0.3402 \end{bmatrix}.$$

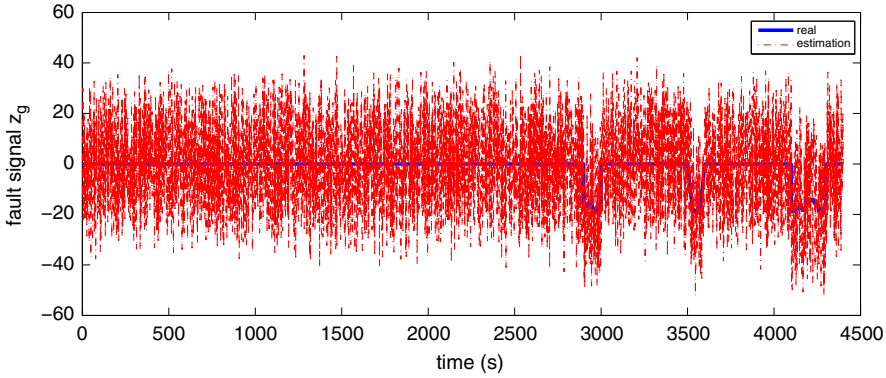

FIGURE 12 Fault signal z_g (real vs estimation). [Colour figure can be viewed at wileyonlinelibrary.com]

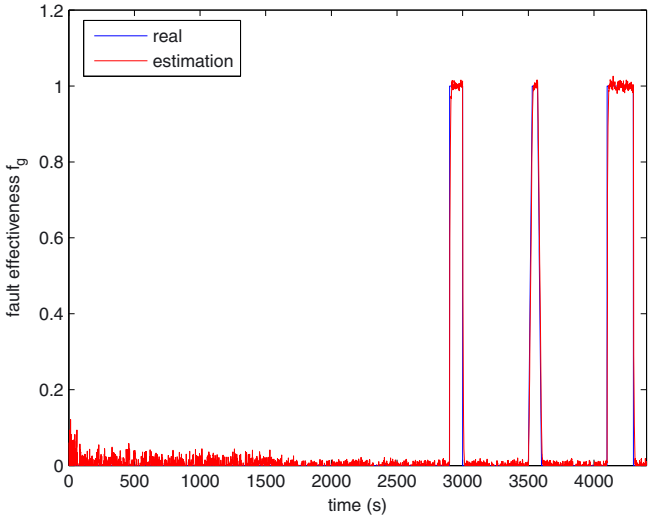

FIGURE 13 Fault effectiveness f_g (real vs estimation). [Colour figure can be viewed at wileyonlinelibrary.com]

In order to assess the performance of this observer, an evolution of the signal $f_g(t)$ similar to the one of $f_1(t)$ provided in Equation 75 has been considered, as follows:

$$f_g(t) = \begin{cases} 1, & 2900\ \text{s} < t \leq 3000\ \text{s} \\ \frac{t-3500}{30} & 3500\ \text{s} < t \leq 3530\ \text{s} \\ 1, & 3530\ \text{s} < t \leq 3570\ \text{s} \\ \frac{3600-t}{30}, & 3570\ \text{s} < t \leq 3600\ \text{s} \\ 1, & 4100\ \text{s} < t \leq 4300\ \text{s} \\ 0, & \text{else} \end{cases}. \tag{76}$$

The results shown hereafter refer to a simulation that lasts 4400 seconds, where the inputs $T_r(t)$ and $T_g(t)$ are as shown in Figure 9.

Figure 10 shows the evolution of the state variables $\omega_r(t)$, $\omega_g(t)$, and $\theta_\Delta(t)$ and their estimation. The effectiveness of the designed observer is confirmed by the state estimation errors, which are plotted in Figure 11.

Figure 12 compares the fault signal $z_g(t)$ with its estimation. In this case, the distinction between the effect of the exogenous disturbances and the effect of the fault is not strong enough to motivate the introduction of threshold-based filtering.

Nevertheless, when recursive least squares with a forgetting factor of 0.997 are applied taking into account Equation 18, a satisfactory estimation of the fault effectiveness parameter f_g is obtained, as shown in Figures 13 and 14.

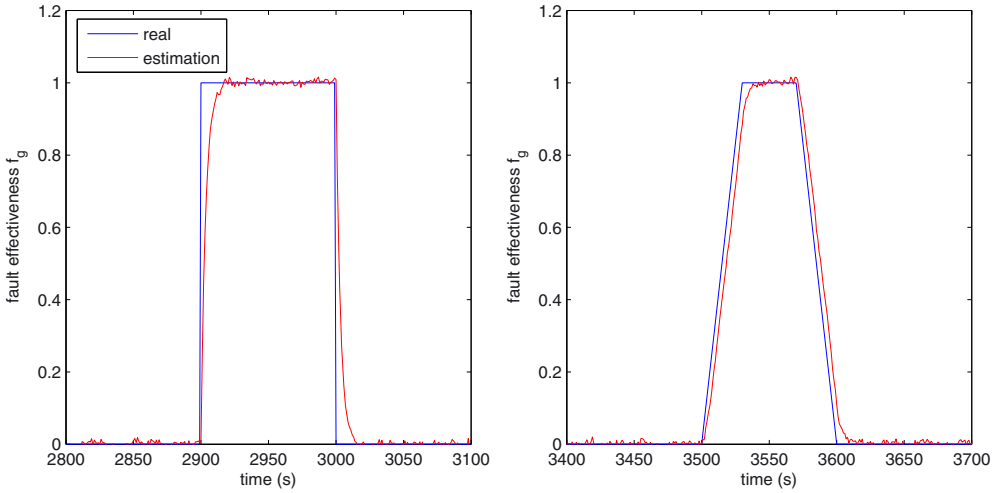

FIGURE 14 Fault effectiveness f_g (real vs estimation, zoom). [Colour figure can be viewed at wileyonlinelibrary.com]

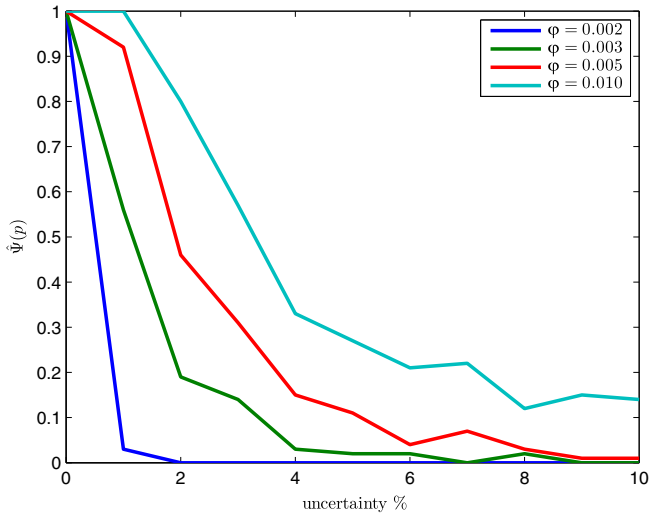

FIGURE 15 Robustness metric estimate $\hat{\Psi}(p)$ for different acceptable MSEs φ. [Colour figure can be viewed at wileyonlinelibrary.com]

4.3 | Robustness assessment

Finally, to assess the robustness of the designed PFE in the presence of model-reality mismatch, the robustness metric described in Section 3.4 has been calculated using extensive Monte Carlo simulations for different ranges of possible parametric uncertainty. The robustness assessment presented hereafter considers uncertainty in the drive train subsystem's parameters: B_g, B_r, J_r, K_{dt}, η_{dt}, B_{dt}, and J_g. For each of these parameters, the uncertainty has been modeled using independent continuous uniform distributions with semilengths equal to a certain percentage of the parameters' nominal values. The Monte Carlo simulations have been performed to obtain $\sigma_{\hat{\Psi}} = 0.05$, which, according to Equation 74, corresponds to $M = 100$.

Figure 15 shows the robustness metric estimate $\hat{\Psi}(p)$ for different acceptable MSEs φ. As expected, to a lower φ (stricter specification) corresponds a lower $\hat{\Psi}(p)$. Also, when the parametric uncertainty increases, the robustness metric decreases (this is not completely true for the robustness metric estimates because of the limited number of Monte Carlo simulations). Using plots as the ones in Figure 15, it is possible to analyze the effects of uncertainty on the performance of the estimator and compare different PFEs. Notice that a similar assessment can be performed for the PFE corresponding to faults in the pitch subsystem.

5 | CONCLUSIONS

This paper has presented a combined adaptive and parameter estimation scheme and its application to the fault estimation of a wind turbine benchmark. In the proposed approach, a set of possible faults affecting the dynamics of the wind turbine are

described. From the model of the system including the considered faults, the proposed estimation scheme has been developed. It is assumed that process disturbances and sensor noises are bounded in an ellipsoid, and hence, its design is realized within the quadratic boundedness framework. A robustness metric that can be used for analyzing the performance in the presence of model-reality mismatch has been proposed, along with a Monte Carlo strategy for obtaining a robustness metric estimate with some desired bound on the standard deviation. Later, the proposed method has been applied to a well-known wind turbine benchmark. From the obtained results, covering a set of predefined fault scenarios, a satisfactory performance of the proposed scheme was assessed, which recommends its application to practical wind turbine installations. The proposed approach works under the assumption that only process faults affect the wind turbine. It is worth noting that the presence of sensor faults could prevent successful joint state and fault estimation. Hence, an important line of future research is to extend the proposed approach to increase its robustness against simultaneous process and sensor faults. Further research will focus on extending the proposed scheme to nonlinear systems using linear parameter–varying or Takagi-Sugeno approaches and integrating it with an FTC scheme dedicated to wind turbines.

ACKNOWLEDGMENTS

This work has been funded by the National Science Centre in Poland under grant 2013/11/B/ST7/01110, by the Spanish Ministry of Science and Technology through the project Health-Aware and Resilient Control of Critical Infrastructures and Complex Systems of the Comisión Interministerial de Ciencia y Tecnología (Reference: DPI2014-58104-R), by L′Agència de Gestió d′Ajuts Universitaris i de Recerca through contract FI-DGR 2015 (Reference: 2015FI_B2 00171), by the Direcció General de Recerca of Generalitat de Catalunya (SAC group Reference 2014/SGR/374), and by the Research Council of Norway through the Centers of Excellence funding scheme (project number 223254 - Centre for Autonomous Marine Operations and Systems, Norwegian University of Science and Technology). Damiano Rotondo also acknowledges that part of this work was carried out during the tenure of an ERCIM Alain Bensoussan Fellowship programme.

REFERENCES

1. Odgaard PF, Stoustrup J, Kinnaert M. Fault tolerant control of wind turbines - a benchmark model. Paper presented at: Proceedings of the 7th IFAC Symposium on Fault Detection, Supervision and Safety of Technical Processes (SAFEPROCESS09); 2009; Barcelona, Spain.
2. Odgaard PF, Johnson KE. Wind turbine fault detection and fault tolerant control - an enhanced benchmark challenge. Paper presented at: 2013 American Control Conference; 2013; Washington DC, USA.
3. Odgaard PF, Stoustrup J, Kinnaert M. Fault-tolerant control of wind turbines: A benchmark model. *IEEE Trans Control Syst Technol*. 2013;21(4):1168-1182.
4. Johnson KE, Fleming PA. Development, implementation, and testing of fault detection strategies on the National Wind Technology Center's controls advanced research turbines. *Mechatronics*. 2011;21(4):728-736.
5. Hameed Z, Hong Y, Cho Y, Ahn S, Song C. Condition monitoring and fault detection of wind turbines and related algorithms: A review. *Renew Sustain Energy Rev*. 2009;13(1):1-39.
6. Odgaard PF, Stoustrup J. Results of a wind turbine FDI competition. *IFAC Proc Vol*. 2012;45(20):102-107.
7. Esbensen T, Sloth C. Fault diagnosis and fault-tolerant control of wind turbines [Master's thesis]. Aalborg, Denmark: Aalborg University; 2009.
8. Chen W, Ding SX, Haghani A, Naik A, Khan AQ, Yin S. Observer-based FDI schemes for wind turbine benchmark. Paper presented at: Proceedings of 18th IFAC World Congress; 2011; Milano, Italy.
9. Blesa J, Rotondo D, Puig V, Nejjari F. FDI and FTC of wind turbines using the interval observer approach and virtual actuators/sensors. *Control Eng Pract*. 2014;24:138-155.
10. Valente de Bessa I, Martinez Palhares R, Vasconcelos D'Angelo MFS, Chaves Filho JE. Data-driven fault detection and isolation scheme for a wind turbine benchmark. *Renew Energy*. 2016;87(1):634-645.
11. Kościelny J, Syfert M, Rostek K, Sztyber A. Fault isolability with different forms of the faults–symptoms relation. *Int J Appl Math Comput Sci*. 2016;26(4):815-826.
12. Seybold L, Witczak M, Majdzik P, Stetter R. Towards robust predictive fault–tolerant control for a battery assembly system. *Int J Appl Math Comput Sci*. 2015;25(4):849-862.
13. Sloth C, Esbensen T, Stoustrup J. Robust and fault-tolerant linear parameter-varying control of wind turbines. *Mechatronics*. 2011;21:645-659.
14. Badihi H, Zhang Y, Hong H. Fuzzy gain-scheduled active fault-tolerant control of a wind turbine. *J Franklin Inst*. 2014;351(7):3677-3706.
15. Kamal E, Aitouche A, Abbes D. Robust fuzzy scheduler fault tolerant control of wind energy systems subject to sensor and actuator faults. *Int J Electr Power Energy Syst*. 2014;55:402-419.
16. Simani S, Castaldi P. Active actuator fault-tolerant control of a wind turbine benchmark model. *Int J Robust and Nonlinear Control*. 2014;24(8-9):1283-1303.
17. Shaker M, Patton RJ. Active sensor fault tolerant output feedback tracking control for wind turbine systems via T-S model. *Eng Appl Artif Intel*. 2014;34(1):1-12.

18. Shi F, Patton R. An active fault tolerant control approach to an offshore wind turbine model. *Renew Energy*. 2015;75:788-798.
19. Schulte H, Gauterin E. Fault-tolerant control of wind turbines with hydrostatic transmission using Takagi-Sugeno and sliding mode techniques. *Annu Rev Control*. 2015;40:82-92.
20. Chen J, Patton RJ. *Robust Model-Based Fault Diagnosis for Dynamic Systems*. Kluwer Academic Publishers; 1999; New York, USA.
21. Bianchi FD, De Battista H, Mantz RJ. *Wind Turbine Control Systems*. New York, NY, USA: Springer-Verlag; 2007.
22. Burton T, Sharpe D, Jenkins N, Bossanyi E. *Wind Energy Handbook*. New York, NY, USA: Wiley; 2008.
23. Munteanu I, Bratcu AI, Cutululis NA, Caenga E. *Optimal Control of Wind Energy Systems - Towards a Global Approach*. New York, NY, USA: Springer-Verlag; 2008.
24. Simani S. Advanced issues of wind turbine modelling and control. *J Phys: Conf Ser*. 2015;659(1):1-20.
25. Burton T, Sharpe D, Jenkins N, Bossanyi E. *Wind Energy Handbook*. John Wiley & Sons Ltd; 2002; West Sussex, England.
26. Hudecz A, Koss H, Hansen M. Ice accretion on wind turbine blades. Paper presented at: Proceedings of the 15th International Workshop on Atmospheric Icing of Structures (IWAIS XV); 2013; Newfoundland and Labrador, Canada.
27. Merritt HE. *Hydraulic Control Systems*. John Wiley & Sons, Inc.; 1967; New York, USA.
28. Johnson KE, Pao LY, Balas MJ, Fingersh LJ. Control of variable-speed wind turbines: standard and adaptive techniques for maximizing energy capture. *IEEE Control Syst*. 2006;26(3):70-81.
29. Alessandri A, Baglietto M, Battistelli G. Design of state estimators for uncertain linear systems using quadratic boundedness. *Automatica*. 2006;42(3):497-502.
30. Ding B. Constrained robust model predictive control via parameter-dependent dynamic output feedback. *Automatica*. 2010;46(9):1517-1523.
31. Ding B. Dynamic output feedback predictive control for nonlinear systems represented by a Takagi–Sugeno model. *IEEE Trans Fuzzy Syst*. 2011;19(5):831-843.
32. Laraba MT, Olaru S, Niculescu SI, et al. Guide on set invariance for delay difference equations. *Annu Rev Control*. 2016;41:13-23.
33. Scherer CW, Gahinet P, Chilali M. Multi-objective output feedback control via LMI optimization. *IEEE Trans Autom Control*. 1997;42(7):896-911.
34. Jiang J, Zhang Y. A revisit to block and recursive least squares for parameter estimation. *Comput Electr Eng*. 2004; 30(5):403-416.
35. Hayes MH. *Statistical Digital Signal Processing and Modeling*. John Wiley & Sons, Inc.; 1996; New York, USA.
36. Marrison CI, Stengel RF. Robust control system design using random search and genetic algorithms. *IEEE Trans Autom Control*. 1997;42(6):835-839.
37. Witczak M, Pretki P. Design of an extended unknown input observer with stochastic robustness techniques and evolutionary algorithms. *Int J Control*. 2007;80(5):749-762.
38. Bartys M, Patton R, Syfert M, de las Heras S, Quevedo J. Introduction to the DAMADICS actuator FDI Benchmark Study. *Control Eng Pract*. 2006;14(6):577-596.
39. Doucet A, de Freitas N, Gordon N. *Sequential Monte Carlo Methods in Practice*. New York, NY: Springer-Verlag; 2001.